# Enhancing the Properties of Styrene-Butadiene Rubber by Adding Borax Particles of Different Sizes

***Habeeb, Salih A.*+; Hasan, Ali S.***

*Department of Polymers Engineering and Petrochemical Industries, Faculty of Materials Engineering, University of Babylon, Al-Hilla City, IRAQ*

***Ţălu, Ş.***

*The Directorate of Research, Development and Innovation Management (DMCDI), Technical University of Cluj-Napoca, 15 Constantin Daicoviciu St., Cluj-Napoca, 400020, Cluj County, ROMANIA*

***Jawad, Akram J.***

*Department of Polymers Engineering and Petrochemical Industries, Faculty of Materials Engineering, University of Babylon, Al-Hilla City, IRAQ*

**ABSTRACT:** *In this research study, borax particles with different average sizes (1.25, 0.75, 0.60 μ m) were added to a styrene-butadiene rubber compound for reinforcement. This rubber has low mechanical, thermal, and surface properties, as well as low resistance to organic solvents. A laboratory two-roll mill was used at room temperature to add the borax particles to the synthetic rubber, then the rheometer characteristics such as torque, scorch time, and cure time were limited at a temperature of 150°C. The results showed that the torque and CRI (curing rate index) improved by 160% for torque and 600% for CRI respectively, dependent on reducing the particle size from 1.25 μm to 0.6 μm. The surface properties shown by FE-SEM, AFM images, and FT-IR analysis indicated a good dispersion of borax particles with an absence of the aggregates when a low borax particle size of 0.6 μm was used. Furthermore, the properties of tensile strength, elongation at break, and the hardness of the rubber compound were improved by 220% for tensile strength, 37% for hardness, and the reduction in elongation at break improved by 25% depending on the reduction in particle size. On the other hand, the resistance of the rubber compound to flame improved, besides the improvement of the thermal conductivity with decreasing particle sizes. The resistance of the rubber compound to organic solvents, such as toluene, was also improved, which was represented by the properties of swelling, the percentage of swelling index, and the cross-link density with 1.07% for swelling index and $1.3\times10^{-3}$ mole/cm$^3$ for cross-link density.*

**KEYWORDS:** *Borax particle sizes; Mechanical properties; Styrene-butadiene rubber; Surface properties; Swelling index; Thermal conductivity.*

***** *To whom correspondence should be addressed.*
**+** *E-mail*: *salihabbas61@yahoo.com ; drsaleh.abbas@uobabylon.edu.iq*
*1021-9986/2021/5/1616-1629 14/$/6.04*

## INTRODUCTION

Over the past few years, the addition of inorganic compounds to elastomeric materials has attracted considerable attention because of its unique and exclusive benefits in various aspects, such as processability, and economic benefits [1, 2]. The use of filler materials in the rubber industry depends largely on two main factors: the particle size and the surface area of the fillings, which substantially improve the thermal and mechanical properties of elastomers [3, 4, 5].

Styrene-Butadiene Rubber (SBR), a synthetic rubber comprising styrene and butadiene monomers, has characteristics like natural rubber, but low mechanical properties, low oil resistance, and low ozone resistance [6, 7]. Therefore, the phenomenon of strengthening rubber compounds using fillings that have a low particle size gives the best results for improving the physical features of rubber compounds, in addition to reducing the swelling rate of rubber due to the availability of the largest contact area between the surface of fillers and the matrix [8, 9]. In addition, small inorganic fillers, especially nanoparticles, give a greater improvement in specifications such as the resistance of the rubber compound to organic solvents (swelling) as a result of the good dispersion of particles in the rubber matrix [10]. Low particle size also provides a high degree of cross-links with the rubber and positively affects tensile strength, modulus of elasticity, hardness, compression set [6, 11], and the low percentage of swelling [12]. Conversely, at large particle size, the bonding between the surfaces of fillers and the matrix has been found to be weak, therefore the dispersion of fillers is inhomogeneous [4]. It is a well-known fact that reduced particle size can modify the surface properties as it reduces surface roughness, fractional dimensions [13], and surface chemistry [14]. The borax decahydrate ($Na_2B_4O_7 \cdot_{10}H_2O$) is a non-toxic food additive that can be applied as a chemical crossing agent for polyvinyl alcohol. Additionally, it can be added in small amounts to increase the viscoelasticity of polymers. Therefore, the complex compounds formed between borax ions and hydroxyl functional groups of the polymer have a multitude of applications in biochemistry and the pharmaceutical field [15].

Borax is an inhibitor that affects the hydration rate and hardening properties of traditional magnesia-phosphate cement. In addition, the nature and quantity of borax can lead to increasing the temperature; compressive strength, and bonding flexural strength of hardened magnesium, and potassium phosphate cement [16]. *Hu et al*. [17] studied the tribological properties of the nanoparticle magnesium borate and found that the wear resistance was improved and the additive decreased the friction coefficient of the oil. *Alaneme* and *Aluko* [18] studied the production quality and age-hardening behavior of Al 6063/SiC-particulate composites were developed using a borax additive. On the other hand, composites containing basalt, such as borax, improve the thermal properties by increasing the filler-polymer interaction that leads to a decrease in the mobility of the polymer chains and a reduction in the efficiency of the decomposition reaction [19,20], in addition to reducing the rubber flammability [20,21]. The low particle sizes of the borax disperse well compared with high particle sizes in the rubber matrix, which leads to more improvement in thermal, tensile, modulus, and swelling properties of rubber compounds [22]. In recent studies, the 3D surface topography of samples was recorded by Scanning Electron Microscopy (SEM) and Atomic Force Microscopy (AFM) and characterized by stereometric analyses [23-25], fractal [26-28], and multifractal [29-31] methods, as well as by Power Spectral Density (PSD) functions [32].

The novelty of this work is represented by an impact study of the regular borax particle size distribution on the curing, physical and surface properties of styrene-butadiene rubber film, which conformed with stereometric/fractal analyses, calculated according to standard ISO 25178-2: 2012 [33].

## EXPERIMENTAL SECTION

### *Materials and Synthesis*

Styrene-butadiene rubber manufactured by the emulsion technique (e-SBR) was used as a continuous stage for all the composites, with a commercial designation (trade name KER 1500); it was bought from Synthos S.A. Oswiecim, Poland. Borax ($Na_2B_4O_7 \cdot_{10}H_2O$), produced by Eti Maden Works, Turkey was used in powder form with a density of 1.73 g/cm$^3$ and a fusion degree of 743˚C. Carbon black HAF-N330 (high-abrasion furnace black) was obtained from MAKROchem S.A., Lublin, Poland, with the following features: external surface area 76 ± 5 m$^2$/g and average particle size 28-36 nm. Zinc oxide (ZnO) was purchased from Lanxess (Cologne, Germany) with a surface area of 6 m$^2$/g.

***Table 1: Basic formulation of rubber compounds added to the Lab. Mill.***

| No. | Ingredients | Quantity (p. h. r.) | | |
|---|---|---|---|---|
| | | A | B | C |
| 1 | SBR $_{KER\ 1500}$ | 100 | 100 | 100 |
| 2 | Stearic acid (Activator) | 1.0 | 1.0 | 1.0 |
| 3 | Zinc oxide (Activator) | 3.0 | 3.0 | 3.0 |
| 4 | Carbon Black (N330) | 40 | 40 | 40 |
| 5 | Borax (Flame Retardant) | 20 | 20 | 20 |
| 6 | Process oil | 8.0 | 8.0 | 8.0 |
| 7 | MBTS (Accelerator) | 1.0 | 1.0 | 1.0 |
| 8 | TMTD (Accelerator) | 0.5 | 0.5 | 0.5 |
| 9 | Sulfur | 1.5 | 1.5 | 1.5 |

*Note: A = rubber compound content 1.25 μm particle size, B = rubber compound content 0.75 μm particle size, rubber compound content 0.600 μm particle size, p.h.r. = parts per hundred of rubber*

Stearic acid was obtained from J.T. Baker® with specific gravity 0.85, maximum ash content 0.1% at 550°C and maximum volatile matter content 0.5% at 65°C. Insoluble sulfur was obtained from J.T. Baker® with specific gravity 1.57, sulfur content 80 ± 2%, maximum ash content 0.2% at 550°C, and maximum volatile matter content 0.5% at 80°C. 2-Mercaptobenzothiazole (Perkacit MBTS) and Tetramethylthiuram-disulfide (Perkacit TMTD) were obtained from Flexsys B.V.

***Preparation of Rubber Specimens***

The SBR masterbatch was prepared using a 6-inch dual-roll mill (Bridge, UK) operating with a friction factor of 1.1, while the rotational velocity of the faster roll was 20 RPM. The process took place at about 50°C based on the ASTMD 15-627 for the production of a uniform 2 mm-thick rubber sheet according to the basic formulation of rubber compounds illustrated in Table 1.

***Vulcanization Process***

The curing properties of the various components were tested at 150°C with an MV-ODR-PROPERTIES rheometer (Micro Vision Enterprises, India) according to ASTM D2705. The Cure Time (TC) and the Scorch Time (TS) of the components are shown in Table 2. The experimental results confirmed that the optimum cure time was 90% of the total Cure Time (TC) was determined at (TC90) according to ISO 6502-2:2018 testing standard at a temperature of 150°C. The rubber compounds were cured in the laboratory of the Department of Polymers Engineering and Petrochemical Industries using an XLB-D 350 × 350 electrically heated press (Huzhou, East Machinery, China) at 150°C with the optimum cure time (TC90) under a pressure of 10 Map.

***Testing of the Surface Parameters***

FE-SEM images of the samples after vulcanization were taken using a Field Emission Scanning Electron Microscope (MIRA 3 TESCAN) with image magnification of 5 μm, 10.7 Kx with high voltage of 30 Kv for detecting the dispersion of the borax particles in the matrix of rubber. The reinforcement of the surface micro-texture of SBR with different borax particle sizes (such as 1.25, 0.75, and 0.60 μm), had been detected using Atomic Force Microscopy (AFM) with contact mode, under the following conditions:

a) Single-crystal silicon VIT-P-C-A / 15 cantilever with Al reflective side coating, of which the length, width, and thickness were 450 μm, 50 μm, and 2.5 μm respectively.

b) The typical resonant frequency and typical force constant were 16 kHz and 0.3 N/m.

c) The scanning rate was 10 mm per minute. Images of the rubber film surfaces were acquired by Scanning Probe Microscopy (SPM) and analyzed with BY3000 SPM 2.9 software, according to the standards ISO 25178-2: 2012 and ASME B46.1 to obtain the analyses of the 3D surface microtexture.

***Fourier Transform InfraRed (FT-IR) spectroscopy analysis***

The chemical bonding between the borax decahydrate particles and SBR for the production of the SBR-Borax decahydrate composite was detected using an IR Affinity-1, supplied by SHIMADZU, JAPAN.

In addition, the 3 mg from the sample produced was mixed with potassium bromide at a ratio of 1:100, with a scan range of 4000–400 $cm^{-1}$, scan resolution 16 $cm^{-1}$, and 15 scans.

***Mechanical and thermal tests***

The tensile inspection was carried out on dumbbell samples according to the ASTM D 412 using an Electronic Universal Testing Machine TIME WDW-5E (Time Group Inc., China). Dumbbell specimens with a thickness of 2 mm were cut off from the molded layers using a Wallace die cutter. The speed test was set at 500 mm/min at 25 ± 3°C, and five specimens were used in tests for each case. The thermal properties of the vulcanized rubber were studied by measuring the thermal conductivity (k), performed using Lee's disc (Griffin and George), and ablation tests were done with an oxy-acetylene flame in accordance with the ASTM E285-08 standard [34]. In addition, the mass ablation rate was tested to limit the rubber compounds' resistance to the loss of mass by using an oxy-acetylene torch, which can be calculated with the following formula [35]:

$$R_m = \frac{M_1 - M_2}{t} \quad (1)$$

where $R_m$ is the mass ablation rate (g/s); $M_1$ and $M_2$ are the mass of samples before and after testing in the (g), and t is the time of the test in seconds [35]. The hardness of the specimens was tested using a Hardness-meter Shore A tester TH200 (Beijing Time Technology Ltd.) according to the ASTM D2240-02 test method. 5 readings were recorded in different places at room temperature for each specimen. The density of the specimens was tested using a high-precision density tester (GP-1205; Matsu Haku), with a range of 0.001-120 g and an accuracy of 0.0001 $g/cm^3$.

***Testing of the Swelling Parameters***

The swelling properties limit the physical properties of rubber compounds after their immersion in organic solvents. Therefore, it is very important to determine the efficiency of these compounds for resistance to decomposition or dissolving in organic solvents. In this work, the samples were weighed accurately before immersion (initial mass) and after their immersion in a specified amount of toluene for 24 hours (swelling mass). Then the samples were placed in a drying oven at 60°C for 24 hours; following this process, the weight of solvent absorbed by the rubber or the net weight of rubber samples after immersion (de- swollen mass) was determined by weighing the dried samples, then determining the swelling properties according to the following steps:

a) determination of the swelling index ($S_I$) of rubber after immersion in the solvent by the following relation [36]:

$$S_1 = \frac{W_1 - W_2}{W_2} \times 100\ [\%] \quad (2)$$

Where $S_I$ is the swelling index in [%]; $W_1$ and $W_2$ are the swollen and initial mass in (g).

b) Determination of the mole percentage uptake of the solvent $Q_t$ can be defined with the following relation [36]:

$$Q_t = \frac{W_2 - W_1}{W_1 \cdot W_m} \times 100\ [\%] \quad (3)$$

Where $Q_t$ is the mole uptake in [%]; $W_m$ is the solvent molar mass of toluene in (g/mole).

c) Determination of the solubility fraction $S_F$ [%] can be defined with the following relation [36]:

$$S_F = \frac{W_2 - W_3}{W_2} \times 100\ [\%] \quad (4)$$

Where:

$S_F$ is the solubility fraction [%]; $W_2$ and $W_3$ are the initial and de-swollen mass in (g).

d) Measurement of the volume fraction of rubber can be defined with the following relation [37]:

$$V_r = \frac{1}{(1 + P_p / S_p)(W_2 / (W_1 - 1))} \quad (5)$$

Where:

$V_r$ is the volume fraction in a swollen specimen [-]; $S_P$ and $P_P$ are the densities of solvent and polymer samples in $g/cm^3$.

e) Determination of cross-link density per unit volume ($mole/cm^3$) can be defined with the following relation [37]:

***Table 2: Density and curing properties of the rubber sample films produced at 150°C and 12 minutes.***

| [a] (μm) | [b] (mg/cm$^3$) | [c] (min$^{-1}$) | [d] (min) | [e] (min) | [f] (N. m) |
|---|---|---|---|---|---|
| 1.25 | 0.906 | 13.1 | 9.95 | 2.6 | 1.604 |
| 0.75 | 0.958 | 20.9 | 6.68 | 1.9 | 5.05 |
| 0.60 | 1.14 | 100.0 | 3.0 | 2.03 | 4.2 |

*Note: [a] Particle size, [b] Density, [c] Cure rate index (CRI), [d] Optimum cure time ($T_{c90}$), [e] Scorch time ($T_{s2}$), [f] Maximum torque (D Max).*

$$V = -\frac{\ln(1 - V_r) + V_r + \chi \cdot V_r^2}{V_0\left(V_r^{1/3} - \frac{2V_r}{f}\right)} \quad (6)$$

Where $V$ is the crosslink density per unit volume (mole/cm$^3$).

$V_r$ is the volume fraction of rubber in a swollen sample [-].

$V_o$ is the solvent molar volume (for toluene is $V_o$ = 106.9 cm$^3$/ mole).

$f$ is the functionality of crosslinks, f = 4, assuming the formation of a tetra-function crosslink.

$\chi$ is the Flory-Huggins rubber–solvent interaction parameter (0.37 for a sulfur cross-linked SBR-toluene pair) [37].

## RESULTS AND DISCUSSION

### *Curing properties*

Three borax particle sizes (1.25, 0.75, and 0.60 μ m) were added in order to reinforce the SBR compound properties. The results showed that the curing properties such as the torque (N • m) and the curing rate index (CRI) improved when using the low particle size. Moreover, the cross-link density in the rubber compounds was increased; also, the low particle size led to a decrease in optimum cure time at 90% of the total cure time (Tc90) and scorch time (TS2). Therefore, the increase in the curing rate index (CRI) leads to an increase in cure speed, because it is inversely proportional to the difference between (Tc90) and (TS2), according to the following relation [38]:

$$CRI = -\frac{100}{Tc_{90} - TS_2} \quad (7)$$

The above results indicated good interaction between the borax particles and the polymer chains, especially at a low size, which depends on the homogeneity and dispersion of particles in the polymeric matrix, which are displayed in Table 2.

### *Surface parameters*

The regular dispersion of borax particles in the rubber matrix leads to the production of a homogeneous surface of the rubber film without the formation of agglomeration when using small particles such as 0.60 μm, as shown in FE-SEM images with 5 μm, 10.7 Kx, and 30 Kv (see Figure 1c). Furthermore, irregular dispersion in the rubber matrix produces a non-homogeneous surface of rubber film, as shown in the FE-SEM images with 5 μm, 10.7 Kx, and 30 Kv (see Figures 1a and 1b), when using particle sizes of 1.25 μm and 0.75 μm respectively. Therefore, the reduction in borax particle size leads to the improvement of the mechanical properties as a result of high dispersion of particles without the formation of agglomerations [14, 35-41].

On the other hand, Figure 2 shows a depth histogram of AFM images of 3-D surface topography with size (21.385 × 21.385 μm$^2$) and particle distribution chart of rubber films filled with different borax particle sizes. From this figure, it can be seen that the degree of dispersion of particles in the rubber surface and the formation of agglomerations depend essentially on the particle size [14, 42], therefore using the AFM images to measure the surface roughness of thin films [24]. From the AFM images, good dispersion and regular distribution of the borax particle size were detected in the polymer matrix. 90% of the particles were smaller than 1.15 μm, 50% of the particles were smaller than 0.45 μm and 10% of the particles were smaller than 0.1 μm for the average particle size with a standard deviation (SD) of 0.600 ± 0.339 μm, as shown in Figures 2e and 2f. In addition, in the polymer matrix of SBR-borax composite rubber film, 90% of the particles were smaller than 1.5 μm, 50% of the particles were smaller than 0. 5 μm, and 10% of the particles were smaller than 0.1 μm for the average particle size with a Standard Deviation (SD) of 0.750 ± 0.418 μm, as shown in Figs. 2c and 2d. Irregular distribution of particles was detected in the SBR-borax composite in the polymer matrix.

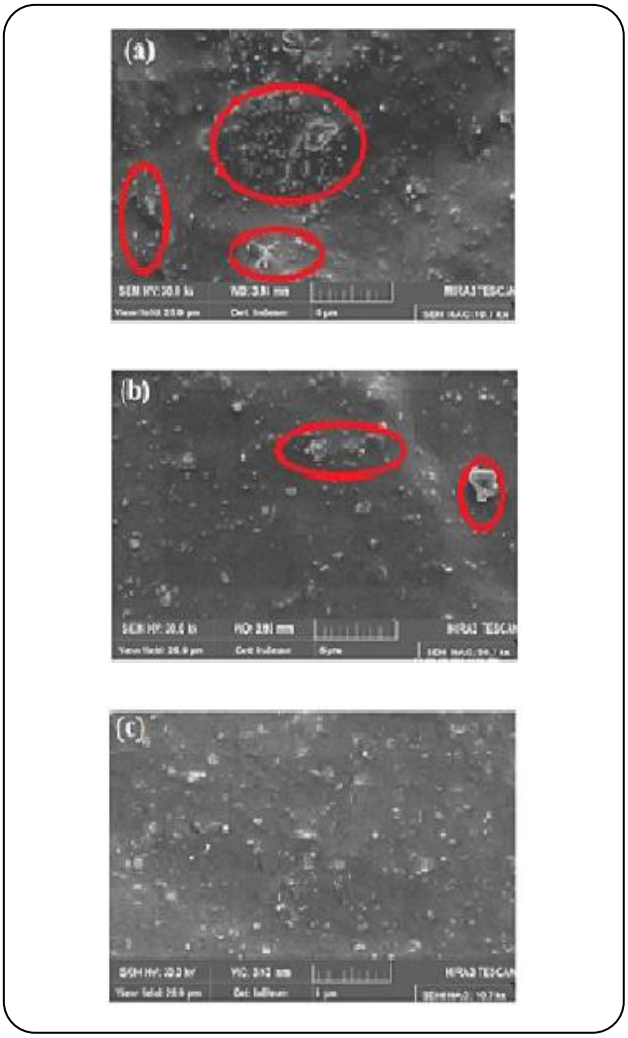


***Fig. 1: FE- SEM micrograph images with 5µm, 10.7 Kx magnification and 30Kv high voltage for rubber compounds filled with particle sizes: (a) 1.25 µm, (b) 0.75 µm and (c) 0.60 µm.***

90% of the particles were smaller than 2.1 µm, 50% of the particles were smaller than 1.1 µm, and 10% of the particles were smaller than 0.400 µm for the average particle size with a standard deviation (SD) of 1.25 ± 0.649 µm, as shown in Figures 2a and 2b.

Therefore, the degree of particle dispersion on the rubber surface and the formation of agglomerations essentially depends on the particle size [14, 42]. The details of surface characterization are based on AFM images obtained by quantitative parameters through ISO 25178-2: 2012 and ASME B46.1-2009 standards (Table 3). The root means square height (Sq) parameter has the highest value for group I (37.6 nm), while the smallest Sq belongs to group III (18 nm), and the middle value is associated with group II (24.6 nm). The surface skewness (Ssk) parameter is positive for all three samples (Ssk > 0), which indicates surfaces with more peaks. The highest value of the Ssk parameter was found for group III (0.0327), a smaller value was found for group II (0.0315) and the lowest value (0.0049) was associated with group I. All three samples have a surface kurtosis (SKU) parameter greater than 1.9. The highest value is 3.01 (for group I, near the Gaussian height distribution), the middle value is 2.84 (for group III) and the lowest values are 1.97 (for group II). The highest value of the ten-point height (S10z) parameter belongs to group III (161 nm), while the lowest value is for group I and group II (79.1 nm). The mean summit curvature (Ssc) value is the lowest (-0.0112 1/nm) for group III and the highest (-0.00073 1/nm) is in the case of group I. The root means square slope (Sdq) parameter has the minimum value (0.0895) for group I, while the highest value belongs to group III (0.372) and the middle value is found for group II (0.117). The highest value of the surface area ratio (Sdr) belongs to group III (5.3%) and the smallest value belongs to group I (0.384%). Therefore, the Sq, Ssk, Sku, and Sdq parameters depend on the surface area ratio (Sdr) [23]; also, the lower fractal dimension leads to a larger surface ratio [25]. The highest values of the Surface-bearing index (Sbi) and the highest core fluid retention index (Sci) parameters are found in group II, while the lowest values are found in group I. The Sbi is 1.58, 3.99, and 1.86 for groups I, II, and III respectively. The highest Sci belongs to the second group (1.62) and the lowest value belongs to the first group (1.54). Group II has the lowest value of the valley fluid retention index (Svi) parameter (0.0273) and the highest value (0.152) is found in group I. The reduced summit height (Spk), the core roughness depth (Sk), and the reduced valley depth (Svk) have the highest values for group I, while the lowest values are found in group III. The density of summits (Sds) of group III has the highest value (3.421/µm2) and the first group has the lowest value (0.0111/ µm2), while the middle value is found in group II (2.151/µm2). The fractal dimensions (average ± standard deviation) were computed and were associated with the corresponding groups as follows: group III displayed the lowest fractal dimension value (2.14 ± 0.01), which corresponds with the most regular topography; group I exhibited the highest value (2.64 ± 0.01); group II exhibited the middle D value (2.21 ± 0.01). The fractional dimension determines the roughness of the surface of

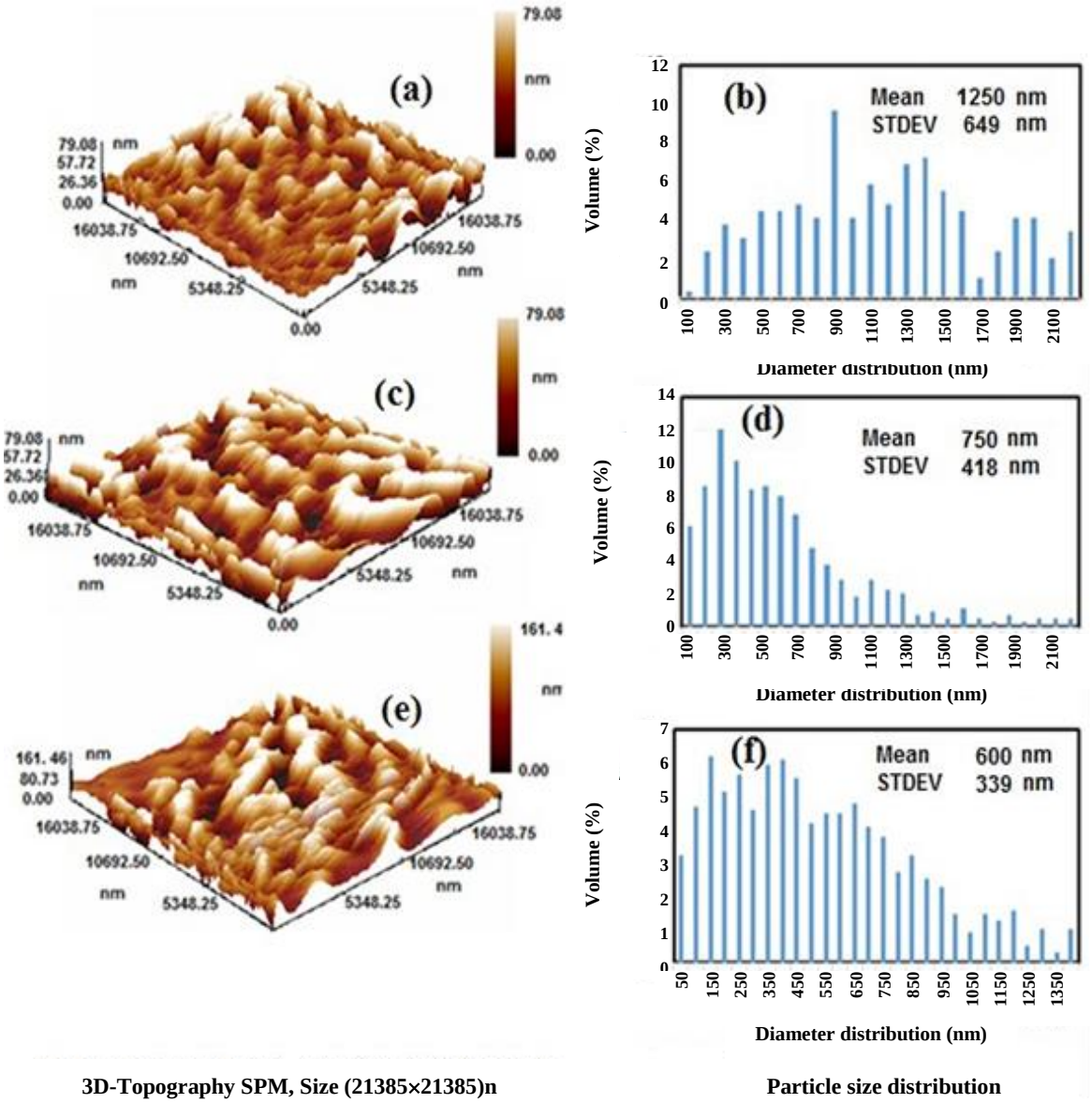


***Fig. 2: Depth histogram of AFM images of 3-D surface topography with size 21.385 × 21.385 μm² at (a, c, e); particle distribution charts of rubber films filled with different borax particles sizes at (b, d, f).***

the thin films; where the fractal dimension value is closest to two, the film's surface is more smoothly and homogeneously distributed [24, 25].

***Fourier Transform InfraRed (FT-IR) spectroscopy analysis for starch particles***

Fig. 3 illustrates the absorption spectra of (a) SBR films without borax, (b) borax particles, (c) SBR films filled with 1.25 μm borax particles, (d) SBR films filled with 0.75 μm borax particles, and (e) SBR films filled with 0.600 μm borax particles. Table 4 represents the wavenumbers of absorption peaks for vibrational bands of the rubber compounds for different borax particle sizes [43]. The CH stretch and OH groups of borax were represented by the absorption peaks at 2931 $cm^{-1}$ The FT-IR absorption peaks of borax at 2931 $cm^{-1}$, which represented the OH groups in borax and the hydrogen bonding between these groups. The FT-IR absorption spectra of SBR exhibited an absorption peak at 2846 $cm^{-1}$, which represented the stretching vibration of the -$CH_2$ and the C=C stretching bonds of the aromatic ring at 1620 $cm^{-1}$. These FT-IR spectra were reported in the literature [44-47],

***Table 3: Statistical parameters for samples with rubber films filled with different borax particle sizes.***

| Statistical parameter | Symbol | Group I | Group II | Group III |
|---|---|---|---|---|
| | | 1.25 μm | 0.75 μm | 0.60 μm |
| ▪ Amplitude parameters | | | | |
| Arithmetic mean height | Sa [nm] | 29.2 | 20.6 | 13.8 |
| Root mean square height | Sq [nm] | 37.6 | 24.6 | 18 |
| Surface skewness | Ssk [-] | 0.0049 | 0.0327 | 0.0315 |
| Surface kurtosis | Sku [-] | 3.01 | 1.97 | 2.84 |
| Ten point height | S10z [nm] | 79.1 | 79.1 | 161 |
| ▪ Hybrid parameters | | | | |
| Mean summit curvature | Ssc [1/nm] | -0.00073 | -0.0029 | -0.0112 |
| Root mean square slope | Sdq [1/nm] | 0.0895 | 0.117 | 0.372 |
| Surface area ratio | Sdr [%] | 0.384 | 0.652 | 5.3 |
| ▪ Functional parameters | | | | |
| Surface bearing index | Sbi | 1.58 | 3.99 | 1.86 |
| Core fluid retention index | Sci | 1.54 | 1.62 | 1.58 |
| Valley fluid retention index | Svi | 0.152 | 0.0273 | 0.139 |
| Reduced summit height | Spk [nm] | 37.7 | 19.7 | 18.5 |
| Core roughness depth | Sk [nm] | 81 | 68.8 | 37.2 |
| Reduced valley depth | Svk [nm] | 47.4 | 35.2 | 25.2 |
| ▪ Spatial parameters | | | | |
| Density of summits | Sds [1/μm$^2$] | 0.011 | 2.15 | 3.42 |
| ▪ Fractal parameters | | | | |
| Fractal dimension | D | 2.5±0.01 | 2.21±0.01 | 2.14±0.01 |

** Statistically significant difference for all values: P < 0.05.*

as shown in Figs. 3a and 3b. At low sizes, the absorption peaks detected led to good dispersion and a large contact surface area between the borax particles and polymer chains. On the other hand, the C-H bend observed at around 771 cm$^{-1}$ and the O–H stretching borax particles revealed characteristic vibration from the hydroxyl groups and hydrogen bonds measured at 3471 and 3479 cm$^{-1}$ for 1.25, 0.75, and 0.6 μm respectively. In addition, the borax particles appeared at 1373 cm$^{-1}$, which represented the stretch vibration of the B−O group for 0.75 and 0.6 μm [22, 48].

In addition, the peak at around 2862 cm$^{-1}$ represents the CH stretching of the CH2 group; this result is approximately the same as that reported in previous literature. The above peak is apparent in the 0.6 μm particles and was absent in the other sizes. This result is confirmed by a strong relationship between the surface contact area of the borax particles and the polymer chains and good dispersion of particles in the matrix, which causes a shift in the absorption peaks, as shown in Fig. 4e. Moreover, in the borax particles measuring 0.6 and 0.75 μm, peaks in the spectrum were observed at about 1056, 2029, 2121, 2553, and 2862 cm$^{-1}$, which represent C-O, N=C, C≡C, S-H, and -CH- bonds, respectively. Figure 3d and Figure 3e show that these peaks were absent in the case of large particle sizes (1.25 μm). In addition, the absorption band at 933 cm$^{-1}$ for the particle sizes 0.6 and 0.75 μm is due to the bending vibration of O-H groups.

***Table 4: Shifts in the FTIR absorption peaks for SBR film filled with various borax particle sizes.***

| Bands | Wavenumber $cm^{-1}$ | | | Assignments |
|---|---|---|---|---|
| | A | B | C | |
| 700 -600 | 601 | 609 | 617 | C-H bend |
| 1110 -1000 | 111 | 1056 | 1064 | Si-OR (broad) |
| 1200 -1050 | 111 | 1056 | 1064 | C=S thiocarbonyl |
| 3000 -2850 | 2924 | 2931 | 2931 | CH stretch, OH, -CH2- |
| 3500 -3200 | 3471 | 3471 | 3479 | H-bonded |
| 3600 -3400 | 3471 | 3471 | 3479 | O-H stretch |

*(A) SBR films filled with 1.25 µm borax particle size, (B) SBR films filled with 0.75 µm borax particle size, (C) SBR films filled with 0.600 µm borax particle size*

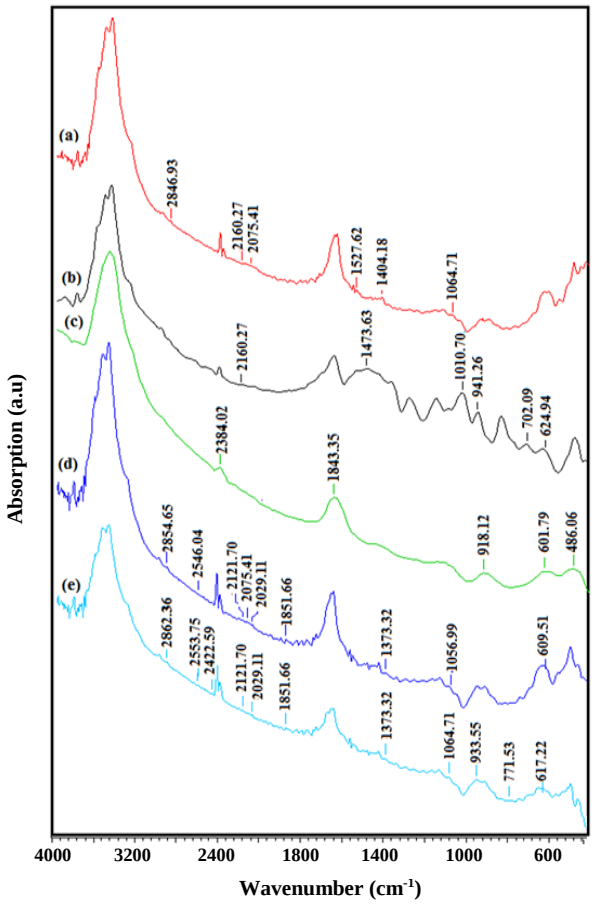


***Fig. 3: FT-IR analysis of (a) SBR films without borax, (b) borax particles, (c) SBR films filled with 1.25 µm borax particles, (d) SBR films filled with 0.75 µm borax particles, (e) SBR films filled with 0.600 µm borax particles***

Conversely, the absorption peaks at 2075 $cm^{-1}$ may be due to the vibration of N=C, which only appeared at 0.75 µm [49]. Therefore, some of the absorption peaks have shifted slightly due to the interaction between the SBR network chains and borax particles, which is dependent on the particle size of borax at 601, 609, and 617 $cm^{-1}$, which represented stretching vibration of the B−C group for 1.25 µm, 0.75 µm, and 0.6 µm borax particle sizes respectively. According to the above results, the low particle size offers the best reinforcement of interaction forces between the borax particles and the polymer matrix, which leads to improvement of the curing, physical and surface properties of the rubber film.

### *Mechanical Properties*

The mechanical properties of the rubber compound were significantly affected by the addition of the borax particles, especially at low particle size. The increase in tensile strength was about 220% and the decline in elongation at break was about 25%, when the particle size was reduced from 1.25 µm to 0.60 µm, as shown in Fig. 4, because the low particle sizes lead to an increase in the homogeneity and interaction with the polymer chains. On the other hand, the surface homogeneity of rubber film without aggregates, which are illustrated in the AFM and SEM images, especially at low particle sizes makes the rubber compound more durable, hard, and difficult to penetrate. As a result, the hardness of rubber films increased from 57.7 Shore A to 79 Shore A with 37% when decreasing the borax particle size from 1.25 µm to 0.60 µm [3, 39, 50].

### *Thermal Behavior of the Rubber Compound*

Borax is an inorganic material that inhibits flame and protects the rubber compounds or reduces the speed of flammability of the rubber compound when it is exposed

to direct flame. Thermal erosion rate tests, such as testing the ablation rate using an oxy-acetylene torch, were conducted on the samples. When the rubber samples were directly exposed to the flames of gases, we notice that the penetration time of flame gases for the thickness of the rubber samples increased with decreasing borax particle size; this result indicated that the ablation rate had the lowest value for the borax particles with a size of 0.6 µm. In other words, this result revealed the homogeneity and the good dispersion of particles in the rubber matrix, which gives a high interaction between the rubber chains and borax particles. Furthermore, this process increases the interconnections that enhance the mechanical properties, as explained in the previous section.

On the other hand, we observed that the oxy-acetylene torch penetration velocity for the rubber specimen thickness will increase with the increasing particle size. Fig. 5 shows the relationship between the ablation rates (the speed of flammability), mass ablation, and the borax particle size. Further, the flames of oxy-acetylene caused an increase in the mass loss of the rubber compound with increasing particle size; this result indicates an increase in the weakness of the cohesion force and heterogeneity with increased particle size. Moreover, the rubber samples filled with the borax particles measuring 0.6 µm lost a small amount of mass when exposed to a gas flame. The physical properties of borax, such as its propensity to disintegrate at high temperatures and its inorganic nature, led to the release of non-flammable gases such as water vapor, which helped to quench the fire by isolating oxygen [51].

Thermal conductivity is a basic property of engineering materials, especially thermal insulators, which reflect the material's ability to transfer heat from molecules with high thermal activity to low thermal activity. The thermal conductivity of the rubber films was tested using Lee's disc (*Griffin* and *George*). These materials were thermal insulators and had low thermal conductivity, especially polystyrene butadiene rubber. The thermal conductivity of the rubber compound depends on the homogeneity and dispersion of the borax particles within the matrix and the temperature used in the process. In Fig. 6, the results in the graph highlight that the thermal conductivity in W/m ˚K for a borax particle size of 0.6 µm had higher values compared to the other particle sizes and original rubber (without fillers) for all temperatures. In addition, the increase in temperature leads to an increase in thermal

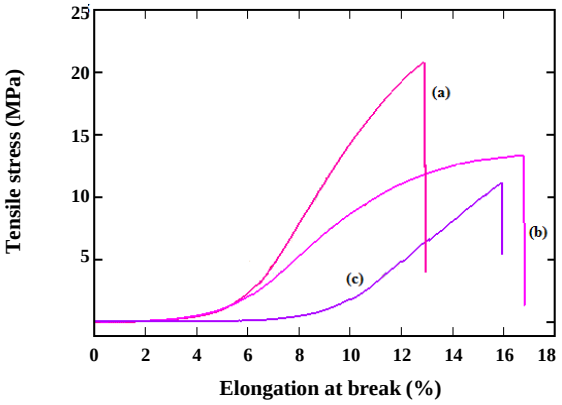


***Fig. 4: The relationship between the tensile stress and the elongation at break for different borax particle sizes: (a) 0.60 µm, (b) 0.75 µm, and (c) 1.25 µm.***

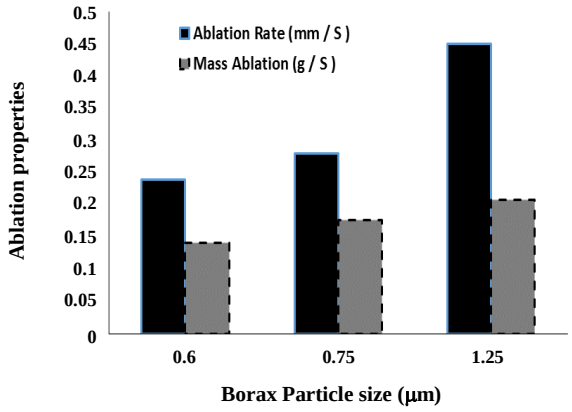


***Fig. 5: The relation between the ablation properties and borax particle size.***

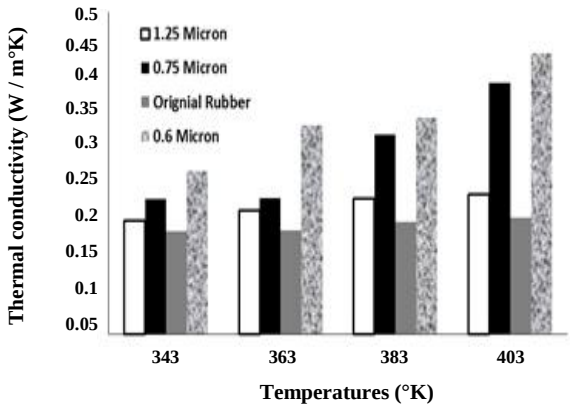


***Fig. 6: The relation between the thermal conductivity of rubber compounds and temperature.***

***Table 5: Swelling parameters results: swelling index, mole % uptake, soluble fraction, rubber volume fraction, and cross-link density for rubber films filled with various borax particle sizes.***

| Average particle size (μm) | $S_I$ (%)[a] | $Q_t$ (%)[b] | $S_F$ (%)[c] | $V_r$ (-)[d] | V (mole/cm$^3$)[e] |
|---|---|---|---|---|---|
| 1.25 | 1.81 | 1.96 | 8.91 | 0.269 | $3.11\times 10^{-4}$ |
| 0.75 | 1.46 | 1.6 | 5.28 | 0.294 | $3.99\times 10^{-4}$ |
| 0.60 | 1.07 | 1.16 | 3.82 | 0.455 | $1.3\times 10^{-3}$ |

*Note: [a] Swelling Index, [b] Mole % Uptake, [c] Soluble Fraction, [d] Rubber Volume Fraction, [e] Cross-Link Density*

conductivity. Therefore, the reduction in the particle size leads to an increase in the packing density and thermal conductivity [52]. Fig. 6 highlights the thermal conductivity of rubber samples for various borax particle sizes in comparison with the original rubber.

***Rubber Swelling Parameters***

Table 2 shows the particle packing density of the rubber compound filled with different borax particle sizes. The particle packing density is influenced by low particle size and is a major parameter of filler reinforcement, as it confirms the strong relationship between the filler packing behavior and physical properties of the rubber compound [53]. The SBR compounds become more resistant to chemical corrosion by solvents such as toluene after being reinforced with borax particles. Table 5 highlights the results of the swelling properties after adding different borax particle sizes, including the swelling index (SI %), the mole percentage uptake of the solvent (Qt %), the soluble fraction (SF %), rubber volume fraction (Vr), and cross-link density per unit volume V (mole/cm$^3$).

The swelling index and cross-link densities were 1.07% and $1.3\times10^{-3}$ mole/cm$^3$ for 0.6 μm particles, while the swelling index and the cross-link density at 0.75 and 1.25 μm particle sizes were 1.46%, 1.81%, $3.99\times10^{-4}$, and $3.11\times10^{-4}$, respectively. These results confirmed that the smaller particles were more dispersed in the matrix of the rubber film; the dispersion was regular, the aggregates were not formed in the rubber films (see Figure 1) and the process of corrosion of the rubber compounds by toluene is more difficult. For a particle size of 0.6 μm, higher values of rubber volume fraction and crosslink density were found, which makes the rubber compound more resistant to toluene. At the same time, for the particle size of 1.25 μm, higher values for a soluble fraction were found because the swelling properties depend on the rubber cross-linking density and the type of solvent used. In addition, solvent corrosion was associated with the highest value of large particle size [40].

## CONCLUSIONS

The experimental results confirmed an increase in the curing rate index (CRI), as well as a decrease in the optimum cure time (Tc90) with an increase in maximum torque (D Max), which suggests increased interconnectivity with small borax particles. The FE-SEM images and FTIR analysis indicated good dispersion with an absence of aggregates for low borax particles. The most regular surface (Sq = 13.8 μm) and the most regular topography (D = 2.14 ± 0.01) was found for samples with a borax particle size of 0.60 μm.

Microtexture analysis of AFM micrographs and fractal analysis of the 3D surfaces are complementary techniques that enable more complete characterization of the 3D geometric surface. The mechanical properties of the rubber compound, such as tensile stress and hardness, exhibited an increase with the reduction of the particle size from 1.25 μm to 0.6 μm. On the other hand, elongation at break decreased when the particle size decreased from 1.25 μm to 0.6 μm. The rubber compound becomes stronger and more resistant to organic solvents such as toluene because of the increased interconnectivity caused by the small borax particles. Furthermore, an improvement in the thermal specifications of the rubber compound, such as thermal conductivity, also limited the speed of flammability and mass ablation when the particle size decreased from 1.25 μm to 0.600 μm.

**Conflict of interest**

The authors declare that they have no conflict of interest.

**Nomenclatures**

CRI Curing Rate Index [s-1]

| | |
|---|---|
| Rm | Mass Ablation Rate [g/s] |
| SI | Swelling Index [%] |
| Qt | Mole Uptake [%] |
| SF | Solubility Fraction [%] |
| Vr | Volume Fraction in a Swollen Specimen [-] |
| V | Crosslink Density Per Unit Volume [mole/cm$^3$] |
| SD | Standard Deviation |
| TC | Optimum Cure Time |
| TS | Scorch Time |
| B-O | Borax-Oxygen bond |
| B-C | Borax-Carbon bond |

*Received : Mar.. 1, 2020 ; Accepted : June 15, 2020*

**REFERENCES**

[1] Fan Y., Li Q., Li X., Hee Lee D., Cho U.R., Comparative Study on Carboxylate Styrene Butadiene Rubber Composites Reinforced by Hybrid Fillers of Rice Bran Carbon and Graphite Carbon, *Carbon Lett.*, **27**:72- 80 (2018).

[2] Habeeb S.A., Rajabi L., Dabirian F., Production of Polyacrylonitrile/ Boehmite Nanofibrous Composite Tubular Structures by Opposite-Charge Electrospinning with Enhanced Properties from a Low-Concentration Polymer Solution, *Polym. Compos.*, **41(4)**: 1649-1661 (2020).

[3] Ahmed K., Nizami S.S., Raza N.Z., Mahmood K., Mechanical, Swelling, and Thermal Aging Properties of Marble Sludge-Natural Rubber Composites, *Int. J. Ind. Chem.*, **3(1)**: 21- (2012).

[4] Jovanović V., Budinski-Simendić J., Milić J., Aroguz A., Ristić I., Prendzov S., Korugic-Karasz, L., "The Effect of Filler Particles on the Properties of Elastomeric Materials Based on Different Network Precursors", In Karasz Frank E., "Contemporary Science of Polymeric Materials", American Chemical Society, Valletta, Malta (2009).

[5] Mohammed F.Q., Hasan A.S., Habeeb S.A., Bkeet W.G., Transport Properties and Applications of Graphene Nano-Ribbon-BN, *Test Engineering and Management*, **83**:10998-11002 (2020).

[6] Sisanth K.S., Thomas M.G., Abraham J., Thomas S., "General Introduction To Rubber Compounding" In Thomas S., Maria Hanna J., "Progress in Rubber Nanocomposites", Woodhead Publishing Series in Composites Science and Engineering: Elsevier (2017).

[7] Heideman G., "Reduced Zinc Oxide Levels in Sulphur Vulcanisation of Rubber Compounds; Mechanistic Aspects of the Role of Activators and Multifunctional Additives", Ph.D.Thesis, University of Twente, Enschede, Netherlands ( 2004).

[8] Habeeb S.A., Alobad Z.K., Albozahid M.A., The Effecting of Physical Properties of Inorganic Fillers on Swelling Rate of Rubber Compound: A Review Study, *Journal of University of Babylon for Engineering Sciences (JUBES)*, **27 (1)**: 94104 (2019).

[9] González N., Custal M.D., Rodríguez D., Riba J.R., Armelin E., Influence of ZnO and $TiO_2$ Particle Sizes in the Mechanical and Dielectric Properties of Vulcanized Rubber, *Mater. Res.*, **20(4)**: 1082- 1091 (2017).

[10] Pashaei S., Hosseinzadeh S., Syed A.A., Studies on Coconut Shell Powder and Crysnanoclay Incorporated Acrylonitrile- Butadiene Rubber/Styrene Butadiene Rubber (NBR/SBR) Green Nanocomposites, *Polym. Compos.*, **38(4)**: 727-735 (2017).

[11] Balasooriya W., Schrittesser B., Pinter G., Schwarz T., Conzatti L., The Effect of the Surface Area of Carbon Black Grades on HNBR in Harsh Environments, *Polymers*, **11(1)**: 61- (2019).

[12] Peng Y.K., "The Effect Of Carbon Black and Silica Fillers on Cure Characteristics and Mechanical Properties of Breaker Compounds", MSc. Thesis, University Science Malaysia, Kubang Kerian, Malaysia (2007).

[13] Fang T.H., Jian S.R., Chuu D.S., Nanomechanical Properties of TiC, TiN and TiCN Thin Films Using Scanning Probe Microscopy and Nanoindentation, *Appl. Surf. Sci.*, **228(1-4)**: 365- 372 (2004).

[14] Gravelle A.J., Barbut S., Marangoni A.G., Influence of Particle Size and Interfacial Interactions on the Physical and Mechanical Properties of Particle-Filled Myofibrillar Protein Gels, *RSC Advances*, **5(75)**: 60723- 60735 (2015).

[15] Han J., Lei T., Wu Q., Facile Preparation of Mouldable Polyvinyl Alcohol-Borax Hydrogels Reinforced by Well-Dispersed Cellulose Nanoparticles: Physical, Viscoelastic and Mechanical Properties, *Cellulose*, **20(6)**: 2947- 2958 (2013).

[16] Yang J., Qian C., Effect of Borax on Hydration and Hardening Properties of Magnesium and Potassium Phosphate Cement Pastes, *J Wuhan Univ Technol–Mater. Sci. Ed.*, **25(4)**: 613- 618 (2010).

[17] Hu Z.S., Lai R., Lou F., Wang L., Chen Z., Chen G., Dong J.X., Preparation and Tribological Properties of Nanometer Magnesium Borate as Lubricating Oil Additive, *Wear*, **252(5-6)**: 370- 374(2002).

[18] Alanemea K.K., Alukob A.O., Production and Age-Hardening Behavior of Borax Premixed Sic Reinforced Al-Mg-Si Alloy Composites Developed by Double Stir-Casting Technique, *The West Indian Journal of Engineering (WIJE)*, **34 (1/2)**: 80- 85 (2012).

[19] Alwaan I.M., Hassan A., Piah M.A., Effect of Zinc Borate on Mechanical and Dielectric Properties of Metallocene Linear Low-Density Polyethylene/Rubbers/Magnesium Oxide Composite for Wire and Cable Applications, *Iran. Polym. J.*, **24(4)**: 279- 288 (2015).

[20] Rybiński P., Syrek B., Żukowski W., Bradło D., Imiela M., Anyszka R., Blume A., Verbouwe W., Impact of Basalt Filler on Thermal and Mechanical Properties, as well as Fire Hazard, of Silicone Rubber Composites, Including Ceramizable Composites, *Materials*, **12(15)**: 2432 (2019).

[21] Raslan H.A., Elnaggar M.Y., Fathy E.S., Flame-Retardancy and Physico- Thermomechanical Properties of Irradiated Ethylene Propylene Diene Monomer Inorganic Composites, *J. Vinyl Addit. Technol*., **25(1)**: 59-67 (2019).

[22] Lu H., Ji N., Li M., Wang Y., Xiong L., Zhou L., Qiu L., Bian X., Sun C., Sun Q., Preparation of Borax Cross-Linked Starch Nanoparticles for Improvement of Mechanical Properties of Maize Starch Films, *J. Agric. Food Chem.*, **67(10)**: 2916-2925(2019).

[23] Sobola D., Ţălu Ş., Solaymani S., Grmela L., Influence of Scanning Rate on Quality of AFM Image: Study of Surface Statistical Metrics, *Microsc. Res. Tech*., **80(12)**: 1328-1336 (2017).

[24] Dallaeva D., Ţălu Ş., Stach S., Škarvada P., Tománek P., Grmela L., AFM Imaging and Fractal Analysis of Surface Roughness of AlN Epilayers on Sapphire Substrates, *Appl. Surf. Sci.*, **312**:81-86 (2014).

[25] Shikhgasan R., Ştefan Ţ., Dinara S., Sebastian S., Guseyn R., Epitaxy of Silicon Carbide on Silicon: Micromorphological Analysis of Growth Surface Evolution, *Superlattices Microstruct*., **86**: 395-402 (2015).

[26] Jelčić Ž., Bulatović V.O., Rek V., Marković K.J., Relationship between Fractal, Viscoelastic, and Aging Properties of Linear and Radial Styrene–Butadiene–Styrene Polymer-Modified Bitumen, *J. Elastomers Plast.*, **48(1)**: 14- 46 (2016).

[27] Knápek A., Sobola D., Burda D., Daňhel A., Mousa M., Kolařík V., Polymer Graphite Pencil Lead as a Cheap Alternative for Classic Conductive SPM Probes, *Nanomaterials*, **9(12)**:1756 (2019).

[28] Naseri N., Solaymani S., Ghaderi A., Bramowicz M., Kulesza S., Ţălu Ş., Pourreza M., Ghasemi S., Microstructure, Morphology and Electrochemical Properties of Co Nanoflake Water Oxidation Electrocatalyst at Micro-and Nanoscale, *RSC Advan*ces, **7(21)**: 12923- 12930 (2017).

[29] Ţălu Ş., Stach S., Méndez A., Trejo G., Ţălu M., Multifractal Characterization of Nanostructure Surfaces of Electrodeposited Ni-P Coatings, *J. Electrochem. Soc*., **161(1)**: D44- 47 (2014).

[30] Ţălu Ş., Stach S., Mahajan A., Pathak D., Wagner T., Kumar A., Bedi R.K ., Multifractal Analysis of Drop- Casted Copper (II) Tetrasulfophthalocyanine Film Surfaces on the Indium Tin Oxide Substrates, *Surf. Interface Anal.*, **46(6)**: 393- 398 (2014).

[31] Ţălu Ş., Morozov I.A., Yadav R.P., Multifractal Analysis of Sputtered Indium Tin Oxide Thin Film Surfaces, *Appl Surf Sci.*, **484**:892- 898 (2019).

[32] Jacobs T.D., Junge T., Pastewka L., Quantitative Characterization of Surface Topography Using Spectral Analysis, *Surf. Topogr. Metrol. Prop*., **5(1)**: 013001 (2017).

[33] Specifications G.P., "Surface Texture: Areal—Part 2: Terms, Definitions and Surface Texture Parameters", International Standard ISO 2012:25178- 2.

[34] Pinto J.R., Sanches N.B., Santos R.D., Oliveira J.I., Dutra R.D., Development of Asbestos-Free and Environment-Friendly Thermal Protection for Aerospace Application, *Mater. Res.*, **21(6)**: e20170856 (2018).

[35] Jin X., Fan X., Jiang P., Wang Q., Microstructure Evolution and Ablation Mechanism of c/c and c/c-sic Composites under a Hypersonic Flowing Propane Torch, *Adv. Eng. Mater*. ,**19(11)**: 1700239 (2017).

[36] Ahmed K., Nizami S.S., Raza N.Z., Shirin K., Cure Characteristics, Mechanical and Swelling Properties of Marble Sludge Filled EPDM Modified Chloroprene Rubber Blends, *Adv. Mater. Phys. Chem.*, **2(2)**: 90- (2012).

[37] Wręczycki J., Bieliński D., Anyszka R., Sulfur/Organic Copolymers as Curing Agents for Rubber, *Polymers*, **10(8)**: 870 (2018).

[38] Habeeb S.A., Alobad Z.K., Albozahid M.A., Effect f Zinc Oxide Loading Levels n the Cure Characteristics, Mechanical and Aging Properties of the EPDM Rubber, *International Journal of Mechanical Engineering and Technology (IJMET)*, **10(1)**: 133- 141 (2019).

[39] Kundie F., Azhari C.H., Muchtar A., Ahmad Z.A., Effects of Filler Size on the Mechanical Properties of Polymer-Filled Dental Composites: A Review of Recent Developments, *J. Phys. Sci*., **29(1)**: 141- 165 (2018).

[40] Mishra S., Shimpi N.G., Patil U.D., Effect of Nano CaCO3 on Thermal Properties of Styrene-Butadiene Rubber (SBR), *J. Polym. Res.*, **14(6)**: 449- 459 (2007).

[41] Kilinc M., "Production and Characterization of Boron Based Additives and the Effect of Flame Retardant Additives on Pet-Based Composites", Ph.D., Thesis, Middle East Technical University, Turkey (2009).

[42] Rodríguez H.A., Casanova H., Effects of Silica Nanoparticles and Silica-Zirconia Nanoclusters on Tribological Properties of Dental Resin Composites, *J. Nanotechnol*., **2018**: - (2018). https://doi.org/10.1155/2018/7589051

[43] Kuptsov A.H., Zhizhin G.N., "Handbook of Fourier Transform Raman and Infrared Spectra of Polymers", Elsevier, Amsterdam (1998).

[44] Kiliç M., Karabul Y., Özdemir Z.G., Erdönmez S., Bulgurcuoğlu A.E., Yeşilkaya S.S., Okutan M., İçelli O., Effect of Borax Additive on the Dielectric Response of Polypyrrole, *Bull. Mater. Sci.*, **41(2)**: 52- (2018).

[45] Nagieb Z.A., Nassar M.A., El-Meligy M.G., Effect of Addition of Boric Acid and Borax on Fire-Retardant and Mechanical Properties of Urea Formaldehyde Saw Dust Composites, *Int. J. Carbohydr. Chem.*, **2011**: (2011). doi:10.1155/2011/146763

[46] Rajadesingu S., Arunachalam K.D., Single Step Pulverization Effect of Borax Decahydrate and Boric Acid—a Comparison, *Mater. Res. Express*, **6(9)**: 094009 (2019).

[47] Arayapranee W., Rempel G.L., Effects of Polarity on The Filler-Rubber Interaction and Properties of Silica Filled Grafted Natural Rubber Composites, *J. Polym*., **2013**: (2013). doi.org/10.1155/2013/279529

[48] Song J., Huang Z., Qin Y., Li X., Thermal Decomposition and Ceramifying Process of Ceramifiable Silicone Rubber Composite with Hydrated Zinc Borate, *Materials*, **12(10)**: 1591 (2019).

[49] Al-Emam E., Motawea A.G., Janssens K., Caen J., Evaluation of Polyvinyl Alcohol–Borax/Agarose (PVA–B/AG) Blend Hydrogels for Removal of Deteriorated Consolidants from Ancient Egyptian Wall Paintings, *Heritage Sci.*, **7(1)**: 22- (2019).

[50] Kemaloglu S., Ozkoc G., Aytac A., Thermally conductive Boron Nitride/SEBS/EVA Ternary Composites: Processing and Characterization, *Polym. Compos*. **31(8)**: 1398- 1408 (2010).

[51] Yu L., Cai J., Li H., Lu F., Qin D., Fei B., Effects of Boric Acid and/or Borax Treatments on the Fire Resistance of Bamboo Filament, *BioResources*, **12(3)**: 5296- 5307 (2017).

[52] Zhang S., Cao X.Y., Ma Y.M., Ke Y.C., Zhang J.K., Wang F.S., The Effects of Particle Size and Content on the Thermal Conductivity and Mechanical Properties of $Al_2O_3$/High Density Polyethylene (HDPE) Composites, *eXPRESS Polym. Lett.*, **5(7)**: 581- 590 (2011).

[53] Aghajan M.H., Hosseini S.M., Razzaghi-Kashani M., Particle Packing in Bimodal Size Carbon Black Mixtures and its Effect on the Properties of Styrene-Butadiene Rubber Compounds, *Polym. Test*., **78**: 106002 (2019).